Miniature High-Q Double-Spiral Slot-Line Resonator Filters

Reza Azadegan, *Student Member, IEEE,* and Kamal Sarabandi, *Fellow, IEEE*

***Abstract*—A new class of low insertion-loss miniaturized filters using slot-line resonators is proposed. Miniaturization is achieved by terminating the slot line with a double-spiral inductive termination at both ends. Using this miniaturized resonator, both positive and negative couplings may be realized, and therefore, both standard coupled-line and cross-coupled quasi-elliptic filters are realizable. The unloaded Q of these slot-line filters is considerably higher than that of miniaturized microstrip filters of comparable dimensions due to the inherent higher Q of the slot line. To demonstrate the validity of the design procedures and the performance characteristics, two different types of filters were fabricated and tested. One is a four-pole Chebyshev filter and the other is a quasi-elliptic filter where, in each case, the full-wave simulations show very good agreement with measurements.**

***Index Terms*—Microstrip filters, microwave filters, miniaturized filters, quasi-elliptic filters, slot-line filters.**

I. Introduction

MOBILE wireless systems of various kinds have been the driving force behind substantial research efforts toward miniaturizing RF front ends. High-Q low insertion-loss miniaturized filters are important requirements. A few approaches in the literature address filter miniaturization, among which are the use of lumped-element filters, high temperature superconducting (HTS) filters, bulk acoustic-wave (BAW) filters, and slow-wave distributed resonator filters [1]–[4].

Lumped-element filters can be made very small at lower frequencies. At higher frequencies, however, their extremely small size may result in high insertion loss and possibly low power-handling capacity. To cope with the insertion-loss problem, HTS filters have been proposed. BAW filters also have exceptionally small size and quite good performance, but may be extremely expensive to develop for any new application. These two classes of filters are not further considered in this paper, the subject of which is to introduce a new type of high-Q coiled slot-line resonator with comparison to the microstrip. On the other hand, conventional distributed element filters using coupled transmission-line resonators exhibit superior performance, but are frequently too large.

In order to reach a compromise between size and performance, some compact architectures have been proposed. The size reduction of ordinary microstrip line resonators, for example, was made possible first by employing microstrip stepped-impedance resonators (SIRs) [5], [6] and then by using hairpin-line resonators [7]. A more compact hairpin filter using split-ring resonators with parallel coupled lines was later proposed [8]. This resonator is a capacitively end-loaded hairpin resonator where the loading is implemented by distributed coupled lines. The loaded hairpin resonator, together with the SIR, resulted in an improved hairpin resonator [9]. Incorporating dissimilar resonators in filter designs has also been reported [9].

Another form of resonator, which is similar to the above hairpin resonators, utilizes square open loops [10]. To further reduce size, the open-loop structure can be modified by introducing a narrow capacitive gap at the open end of the loop [11]. The same authors suggested an aperture coupled two-layer filter design using the same type of resonator [12]. Using the two sides of the substrate provides additional miniaturization. In both loaded open-loop and loaded hairpin resonators, electric and magnetic coupling can be implemented, which allows for the flexible design of many structures, such as quasi-elliptic filters.

Slot lines and coplanar waveguides (CPWs) are other important configurations for the realization of resonators and filters. In the early 1970s, slot transmission lines were shown to be a practical configuration for the realization of microwave filters and couplers [13], but more attention has been devoted to CPW filters [14]–[16]. Also known as uniplanar configurations, slot and CPWs are fundamental to many microwave and millimeter-wave integrated circuits [17], [18]. With regard to CPW filter miniaturization, the use of quarter-wave transmission-line resonators, e.g., a $\lambda/4$ CPW hairpin resonator [19], meandered superconducting CPW filters [20], double-surface CPW filters [21], and air-bridge capacitive loadings have been proposed. Additionally, the periodic loading of CPW lines has been suggested to construct a slow-wave transmission line and has been used in the fabrication of a miniature low-pass filter [22].

In contrast, the literature concerning the use of slot lines for filter design and filter miniaturization is rather sparse [23]. The Q of slot-line resonators is higher than that of microstrip resonators of similar dimensions due to the fact that the stored energy in the resonator is confined within a larger volume and that the electric current flows over a wider area, which translates into lower ohmic losses. Actually, slot lines are comparable to suspended substrate strip lines, which also have higher Q than microstrips due to the larger volume occupied by the stored energy.

In this paper, new filter architectures based on a miniaturized slot line with double-spiral inductive terminations are proposed.

Manuscript received December 1, 2003.

The authors are with the Radiation Laboratory, Department of Electrical Engineering and Computer Science, The University of Michigan at Ann Arbor, Ann Arbor, MI 48109-2122 USA (e-mail: azadegan@eecs.umich.edu; saraband@eecs.umich.edu).

Digital Object Identifier 10.1109/TMTT.2004.827044

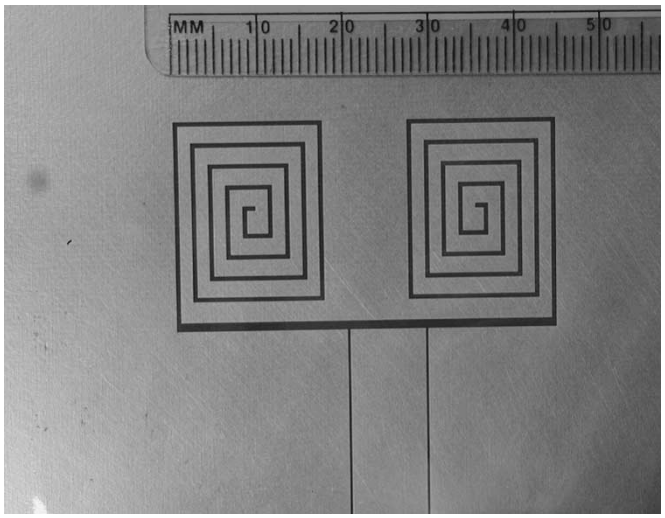

Fig. 1. Proposed miniaturized resonator capacitively coupled at 400 MHz with asymmetric end loadings.

Both electric and magnetic couplings are achievable by appropriate geometric layout of the miniaturized resonators, enabling quasi-elliptic filters to be designed.

II. Miniaturized Slot-Line Resonator Topology

Recently, the authors proposed a highly efficient miniaturized slot antenna using a resonant slot-line geometry [24]. Comparing this slot antenna with its complementary printed strip counterpart shows a considerable increase in the antenna efficiency mainly due to lower ohmic losses [25]. Thus, miniaturized slot-line resonators may be expected to exhibit higher Q than their microstrip versions.

Fig. 1 shows the geometry of the miniaturized slot-line resonator with double-spiral inductive terminations. The very compact inductive end loading is realized by coiled shorted slot lines, each with a length smaller than a quarter-wavelength. This resonator exhibits a superior miniaturization factor and is capable of generating electric, magnetic, and mixed coupling mechanisms.

To assess the performance of the miniature slot-line resonators, a capacitively coupled miniaturized resonator, as shown in Fig. 1, was fabricated on a 0.787-mm-thick Duroid substrate with a dielectric constant of $\epsilon_r = 2.2$ and a loss tangent of $\tan\delta = 0.0009$.[1] The same substrate is used for the rest of the designs presented in this paper to give direct comparisons. A low-permittivity substrate was used to minimize the effects of dielectric loading on miniaturization. The resonator of Fig. 1 is designed to operate at 400 MHz and fits within a rectangular area with dimensions $0.06\lambda_0 \times 0.03\lambda_0$. The unloaded Q can be found using a single-port impedance/admittance measurement technique referred to as the critical-point method [26]. The unloaded Q of the miniaturized resonator at 400 MHz was measured to be $Q_0 \approx 210$, which compares favorably with the Q of miniaturized hairpin resonators [8], while being about an order of magnitude smaller in area.

[1]RT/Duroid 5880, Adv. Circuit Mat. Div., Rogers Corporation, Chandler, AZ.

TABLE I
Effect of the Slot-to-Strip Width (s/w) on the Unloaded Q of the Miniaturized Slot-Line Resonator

s/w	0.2	0.33	0.5	1.0
f_0 [GHz]	2.29	2.37	2.45	2.605
Q_0	120	140	195	173

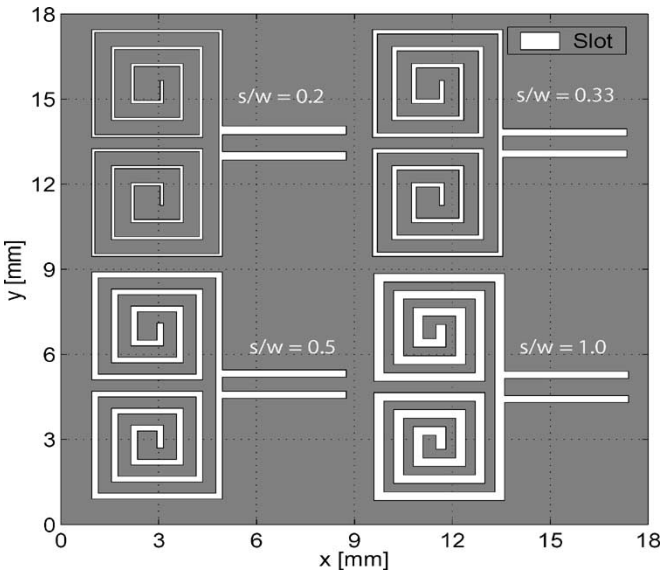

Fig. 2. Miniaturized slot-line resonator topology with different ratios of slot-to-strip width (s/w).

Using the relationship [1]

$$Q = K\, b \sqrt{f} \tag{1}$$

where b is a linear dimension of the resonator, and K is a constant defined as a figure-of-merit, a better comparison can be made between miniature slot-line and microstrip resonators. For microstrip resonators, b is defined as the substrate thickness, while for the slot resonators, b represents the slot width. Invoking (1), the figure-of-merit constant K is found to be $K = 100$ for the miniaturized hairpin resonator [8], and $K = 330$ for the slot-line resonator of Fig. 1.

The ohmic loss of the CPW lines and slot lines is drastically affected by the width of the slot or, equivalently, the impedance of the line [13]. At resonance, the electric current distribution on the ground plane around the slot has a higher concentration near the edges. By making the slot wider, the peak of the current at the edges is reduced, and a smoother current distribution away from the slot edges is obtained. Lower current distribution at the edges translates into lower ohmic losses. In order to obtain the best Q_0, for a given resonator, the width of the slot line may be optimized. Table I compares the unloaded Q of the proposed miniaturized resonator topology with a number of different slot-line widths (see Fig. 2). In this study, the overall size of the resonator is fixed while (s/w), i.e., the ratio of the slot width (s) to the adjacent metallic strip width (w), is varied as a parameter. For the proposed miniaturized double-spiral slot resonator, the width of the metallic strips should be approximately twice the width of the adjacent slots ($s/w = 0.5$). Fig. 3 shows an optimized miniaturized resonator at 2.45 GHz with approximately the same size as the previous resonator relative to the

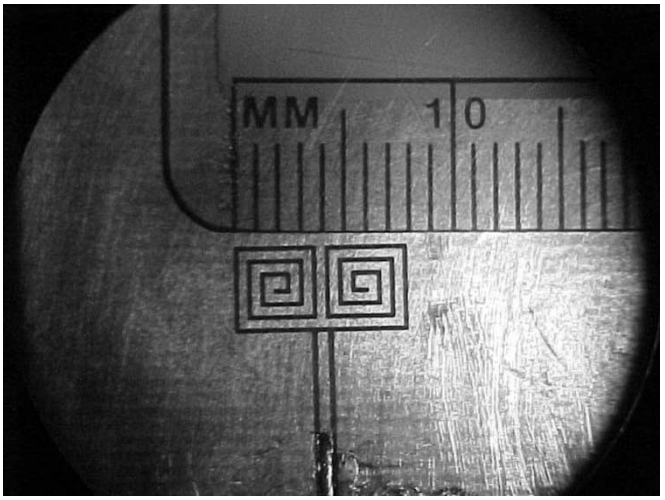

Fig. 3. Optimized miniature resonator at 2.45 GHz.

wavelength, namely, $0.03\lambda_0 \times 0.06\lambda_0$. The unloaded Q is found to be $Q_0 \approx 195$. A comparison of the Q_0 of this resonator with that of the scaled version of the resonator in Fig. 1 (shown in Table I with $s/w = 0.2$) exhibits a considerable improvement due to the effect of slot-line impedance on reducing the ohmic losses of the resonator. The figure-of-merit constant K for the optimized miniature resonator with $(s/w = 0.5)$ at 2.4 GHz can be obtained from (1) as $K = 600$, which is four times higher than that of a half-wave microstrip resonator.

It is worth mentioning that (1) indicates that the Q of a given resonator increases as $\sqrt{f}$. However, there is a limitation on the maximum value of the linear dimension b, which is inversely proportional to frequency. Hence, if one compares resonators having the maximum possible values of b, one can define an available Q, which decreases by the square root of frequency.

To measure the radiation loss of the resonator, it was enclosed in a larger metallic cavity, and its Q was measured to be $Q_0' = 265$. Therefore, the Q due to the radiation loss can be obtained from

$$\frac{1}{Q_{\rm rad}} = \frac{1}{Q_0} - \frac{1}{Q_0'} \tag{2}$$

giving $Q_{\rm rad} \approx 808$. This result indicates that the Q of the resonator is dominated by the ohmic and dielectric losses.

Here, only measurement has been used to identify the quality factor of the proposed resonators since a numerical estimate of Q for the miniaturized resonators does not provide very accurate results. For example, the finite-element method (FEM) would require enormous amounts of memory and extremely small cell sizes due to the very large ratio of fine and coarse features of the structure. On the other hand, full-wave methods based on integral equations [method of moments (MoM)] make use of the Green's function for multilayer structures of infinite extent. Hence, ground planes and substrates of finite size cannot be modeled efficiently. The equivalent magnetic-current method, however, provides a numerically efficient approach for the simulation of slotted structures. In this approach, the tangential electric field over the slot is replaced with an equivalent magnetic current, while the field is assumed to vanish over the ground plane. This assumption implies that the ground plane is a perfect conductor, and therefore, the ohmic loss cannot be modeled in this case. Obviously, the ground plane of the slot-line resonators under study is neither a perfect conductor, nor is it extended to infinity. Despite the aforementioned drawbacks of the integral-equation method, such as [27], it can predict the frequency response of the filters very accurately with the exception of the insertion loss.

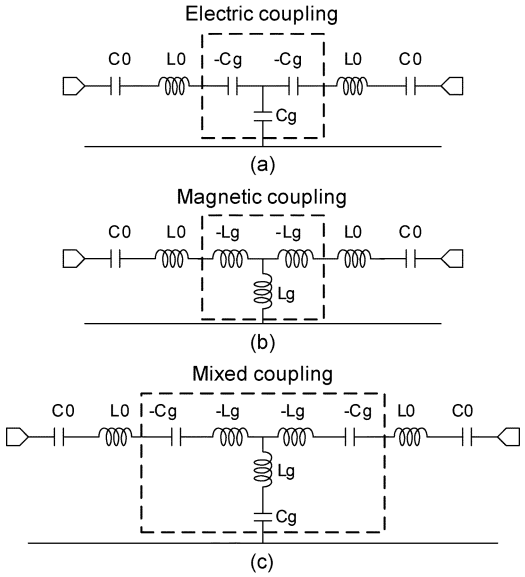

Fig. 4. Equivalent-circuit model of coupled miniaturized resonators exhibiting: (a) electric coupling, (b) magnetic coupling, and (c) mixed coupling.

III. Direct Coupled Four-Pole Filter

To demonstrate the versatility of the proposed miniaturized resonators to design different types of filters, we begin with the design of direct coupled bandpass filters.

A. Coupling Structures

For the case of capacitively coupled miniaturized slot resonators, the resonators have a series equivalent circuit model. Fig. 4 illustrates the equivalent circuit of two coupled miniaturized resonators exhibiting electric, magnetic, and mixed couplings, all realized by an impedance (K) inverter.

In order to realize the desired values for the coupling coefficients, there are differing coupling configurations. In each of these configurations, the coupling coefficients may be extracted using the pole-splitting method [10] in conjunction with full-wave simulations [27]. Given that f_u and f_l are the frequencies at which the S_{21} reaches its peak values, the coupling coefficients can be obtained from

$$k = \frac{f_u^2 - f_l^2}{f_u^2 + f_l^2}. \tag{3}$$

In the case of the pure electric or magnetic couplings whose appropriate circuit models are shown in Fig. 4(a) and (b)

$$k_e = \frac{C_0}{C_g} \text{ (electric coupling)}$$
$$k_m = \frac{L_g}{L_0} \text{ (magnetic coupling)}. \tag{4}$$

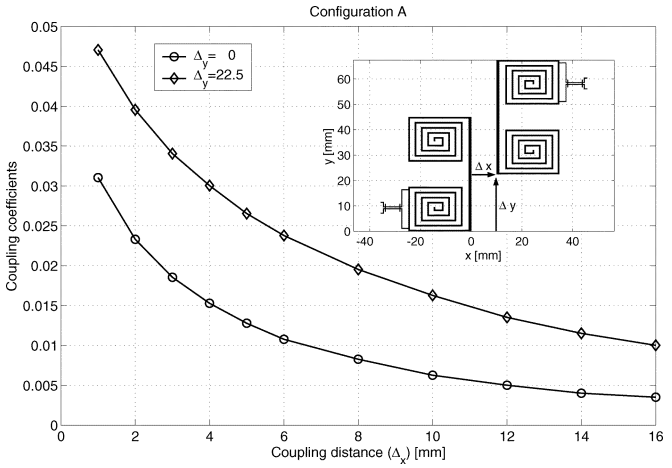

Fig. 5. Extracted coupling coefficients for a back-to-back coupling configuration A as a function of the horizontal separation Δx for two different values of vertical offsets Δy.

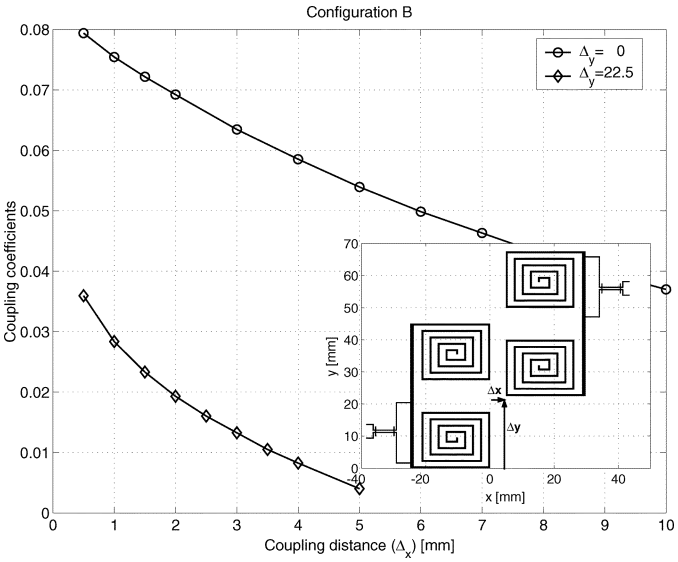

Fig. 6. Extracted coupling coefficients for configuration B (face-to-face arrangement) as a function of horizontal separation Δx for two different values of vertical offsets Δy.

Note that, in the case of electric coupling, the capacitance to ground C_g of the impedance inverter is formed by the relatively wide ground-plane region of length Δx between the two resonators shown in Fig. 5. Since the inverter impedance is $K = 1/(\omega_0 C_g)$, a larger Δx gives a larger C_g, and the inverter impedance becomes smaller. Note that the coupling coefficient is proportional to K in the series representation [28], which is consistent with the looser coupling requirement as C_g and Δx increase. Also note that C_g relates only to the K inverter impedance and is unrelated to the mutual capacitance between the resonators.

Mixed coupling may also be represented by an impedance invertor, as shown in Fig. 4(c). Since usually $C_0 \ll C_g$ and $L_g \ll L_0$, the coupling coefficient for the mixed coupling can be simplified as

$$k_{em} = \frac{L_0 C_0 - L_g C_g}{L_g C_0 - L_0 C_g} \approx \frac{L_g}{L_0} - \frac{C_0}{C_g} = k_m - k_e. \quad (5)$$

Equation (5) indicates that, for mixed coupling, the electric and magnetic coupling are out-of-phase and tend to counteract each other. Examining the mixed coupling more closely, it becomes clear that, at the frequency of $\omega_n = 1/\sqrt{L_g C_g}$, the two resonators in Fig. 4(c) become decoupled, and a zero in the passband is introduced. For dominant electric coupling where $k_e > k_m$

$$\frac{1}{C_g \omega_0} > \omega_0 L_g \Longrightarrow \omega_n > \omega_0 = \frac{1}{\sqrt{L_0 C_0}}. \quad (6)$$

Likewise, when the magnetic coupling is dominant, the zero appears below the passband, i.e., $\omega_n < \omega_0$.

In order to design the first Chebyshev sample design, two different coupling configurations are investigated. These configurations are identified according to the mutual orientation of the two resonators with respect to each other. The first coupling configuration, henceforth referred to as configuration A, is one in which the resonators are positioned back-to-back, as shown in Fig. 5. The coupling coefficient (k) is calculated from (3) and is plotted as a function of the horizontal distance between the resonators (Δx) for two different values of vertical offsets (Δy). Fig. 6 shows a face-to-face coupling arrangement and its calculated coupling coefficients, henceforth referred to as configuration B.

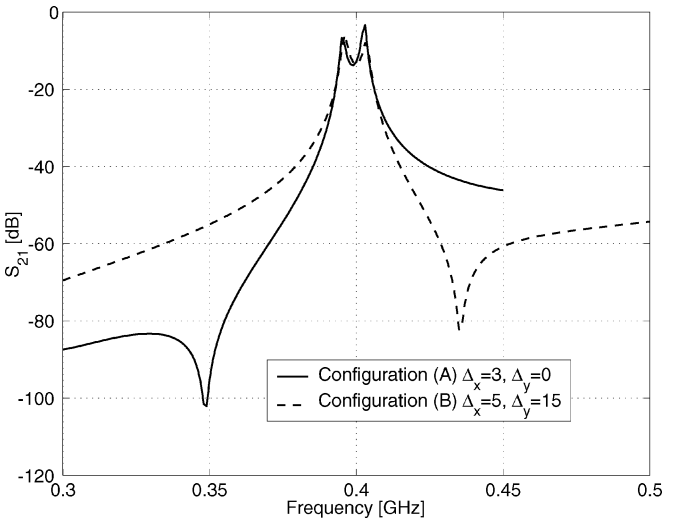

Fig. 7. Comparison between dominantly magnetic (configuration A) and dominantly electric (configuration B) for the same overall coupling coefficient. (Note the locations of zeros.)

Since the proposed resonators are very compact and in close proximity to each other, the coupling mechanism is complex. The external coupling topology also has a significant effect on the nature of the couplings, and thus, each case should be studied separately. Fig. 7 shows the pole-splitting phenomenon in the S_{21} responses of the two coupling configurations. The coupling parameters for configuration A were set to $\Delta x = 3$ mm and $\Delta y = 0$, and for configuration B, to $\Delta x = 5$ mm and $\Delta y = 15$ mm so as to provide approximately the same coupling value. The S_{21} responses shown in Fig. 7 demonstrate that both structures are coupled through a mixed-coupling mechanism since there is a zero in the transmission. The locations of the zeros, however, are different. For configuration A, $\omega_n < \omega_0$, and thus,

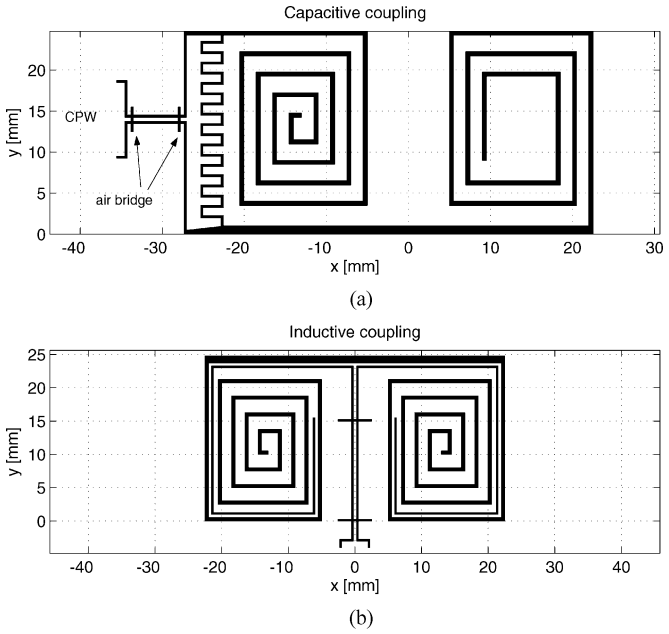

Fig. 8. Two different methods for external coupling. (a) Electric coupling. (b) Magnetic coupling.

magnetic coupling is dominant. For configuration B, $\omega_n > \omega_0$, indicating that the electric coupling is dominant.

Considering configuration A and recalling the fact that the electric-field distribution in a resonant slot line is maximum at the center, electric coupling is maximized when there is no vertical offset between the two resonators, namely, $\Delta y = 0$. However, it is interesting to note that although the electric coupling decreases as Δy increases, the overall coupling increases (see Fig. 5). This behavior indicates that magnetic coupling is dominant and electric coupling counteracts the effect of magnetic coupling in this configuration. This behavior is also consistent with the increasing trend of magnetic coupling as Δy is increased, noting that the electric current linkage (magnetic coupling) from the first resonator to the second one is increased by a factor proportional to Δy.

As for configuration B, shown in Fig. 6, two mechanisms give rise to electric coupling. One is the direct capacitance between the input and output, and the other arises from the electric coupling between the adjacent coiled slot arms. Both of these electric coupling components are inversely proportional to distance (Δx). Similarly, when Δy increases, these components are reduced. Conversely, the electric-current linkage (magnetic coupling) between the two resonators is increased. This argument confirms the fact that both types of couplings are present, and since the overall coupling decreases with an increase in Δy, the magnetic coupling is the one subtracted from the dominant electric coupling.

B. External Coupling

For the miniaturized slot-line resonator, both electric and magnetic external couplings can be realized. Fig. 8(a) and (b) illustrates input and output electric and magnetic couplings, respectively.

Electric coupling can be controlled by the value of the interdigital capacitor inserted between an input or output CPW line and the slot resonator. By changing the gap size and/or finger length of the interdigital capacitor, shown in Fig. 8(a), a wide range of electric external coupling values can be realized. However, note that when the finger length of the capacitor is increased, the resonant slot length is increased, and therefore, the resonant frequency of the structure shifts downward. To alleviate the frequency shift, the size of the resonator must be trimmed in a such a way as to maintain the resonance of the structure intact, which is why one of the inductive terminations in Fig. 8(a) is shorter. In the case of magnetic external coupling, depicted in Fig. 8(b), the length of the CPW coupled line extension controls the magnitude of the external coupling.

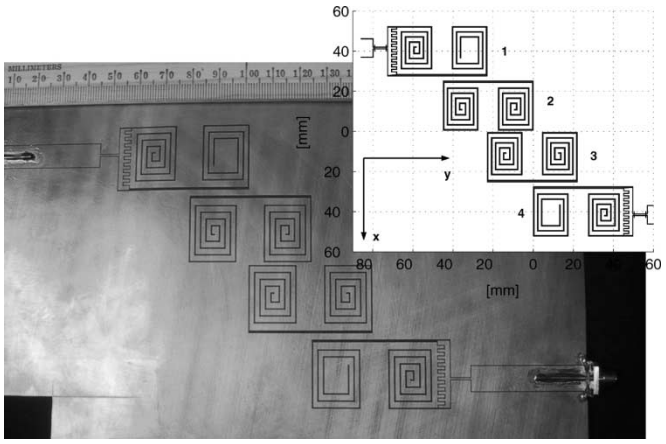

Fig. 9. Photograph and schematic of the miniaturized four-pole Chebyshev filter at 400 MHz.

C. Examples

In order to demonstrate the performance of the proposed miniaturized filters, two examples are considered. In the first example, a four-pole Chebyshev filter with a fractional bandwidth of 5% and 0.25-dB ripple at 400 MHz is designed and shown in Fig. 9. The required coupling coefficients are $k_{12} = k_{34} = 0.0378$ and $k_{23} = 0.0310$, and the external coupling is $Q_{\text{ext}} = 27.565$ [28]. The prescribed coupling coefficients can be realized using the design curves of Figs. 5 and 6. For this design, a fixed vertical offset $\Delta y = 22.5$ mm was chosen in order to obtain a more realizable horizontal offset and also to ensure that nonadjacent resonators do not couple to each other. The horizontal offsets in the first example are found to be $\Delta x_{1,2} = \Delta x_{3,4} = 2.25$ mm and $\Delta x_{2,3} = 0.85$ mm. The area occupied by this filter is $0.22\lambda_0 \times 0.06\lambda_0 = 0.0132\lambda_0^2$. As illustrated in Fig. 10, the measured response of the filter accurately follows the numerical results obtained by a full wave MoM simulation [27].

A frequency shift of less than 0.5% occurs, which can be attributed to the finite size of the ground plane, noting that, in the MoM simulation, an infinite ground plane is assumed. The minimum measured insertion loss for this filter is approximately -1.7 dB, corresponding to a Q of 240. Note that the Q of a miniature microstrip filter of comparable dimensions is less than 70.

The next example considers an inductive mechanism for the external coupling of a four-pole Chebyshev bandpass filter with 3% bandwidth. For this example, an inline resonator design

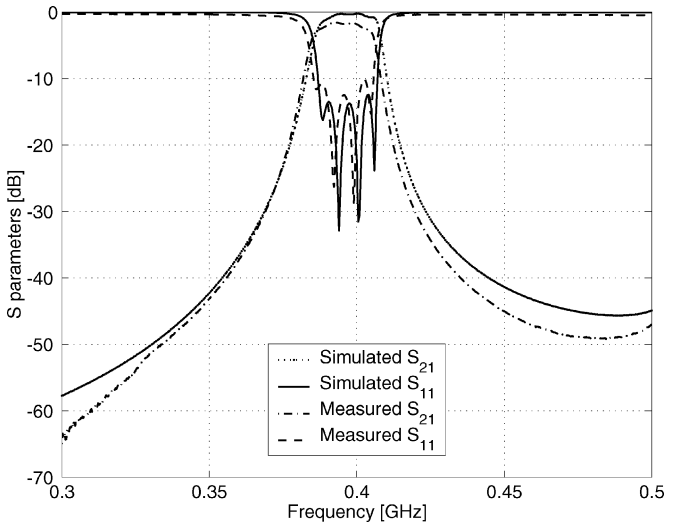

Fig. 10. Comparison between the simulated and measured S-parameters of the filter in Fig. 9.

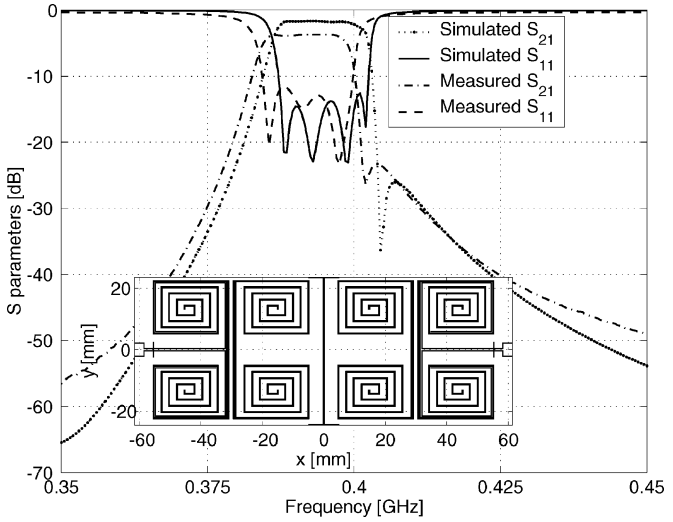

Fig. 11. Layout of a four-pole miniaturized filter with inline resonators at 400 MHz, as well as the comparison between its simulated and measured S-parameters.

($\Delta y = 0$) is used to further reduce the area occupied by the filter. In configuration B, electric coupling is dominant, which produces an excess coupling coefficient. If a short slot line is inserted between two face-to-face resonators, electric coupling can be reduced considerably, and therefore, a much smaller Δx is needed to achieve the prescribed coupling coefficient. Fig. 11 shows the designed filter in which configuration B is modified for further compactness.

The dimensions of this filter are $0.15\lambda_0 \times 0.06\lambda_0 = 0.009\lambda_0^2$. The comparison between the measured and simulated responses is illustrated in Fig. 11. In this example, an insertion loss of -3.7 dB is achieved, which corresponds to the Q of 220. Obviously, due to the modification to coupling configuration B, the zero associated with the mixed coupling now becomes closer to the passband ($\omega_n \rightarrow \omega_0$) and enhances the rejection in the upper band. This observed zero in the rejection band arises from a mechanism different from that of normal quasi-elliptical filters

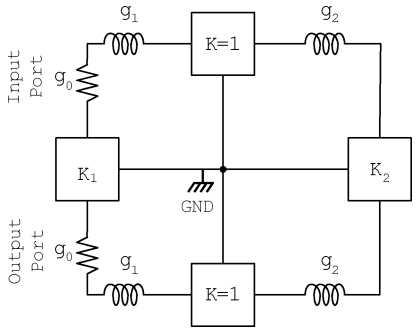

Fig. 12. Schematic of a low-pass prototype quasi-elliptic filter with series elements.

where the passband zeros are the results of the cancellation of multipath signals through different resonators.

IV. Cross-Coupled Miniature Filters

In the RF front end of many wireless devices, quasi-elliptic filters are commonly used because of their compactness and high selectivity. The enhanced out-of-band rejection of elliptic filters is due to the presence of zeros in the filter transfer function created by cross-couplings [29]–[31]. Here, the synthesis of a lumped-element low-pass prototype of a four-pole quasi-elliptic filter is demonstrated, and then, the required coupling coefficients and external couplings are extracted. Different coupling architectures appropriate for the proposed resonator and suitable for realizing the required coupling coefficients, including negative values, will be investigated. Following a procedure similar to the one used in Section III, a typical four-pole cross-coupled filter is designed, fabricated, and tested.

Fig. 12 shows a low-pass prototype for a four-pole cross-coupled filter with series elements. In the above, $g_0 = 1$ represents source and load normalized impedances, and the remaining four unknowns are found following a synthesis procedure outlined in [30].

For the following design example, a filter with a fractional bandwidth of $W = 5\%$ and passband ripple of 0.1 dB is considered. The transmission zero parameter is also set to $a = 2j$, which implies the occurrence of two transmission zeros at $\omega_n = \omega_0(1 \pm W)$. Thus, prototype elements in Fig. 12 are calculated to be $g_1 = 0.9526$, $g_2 = 1.3822$, $K_1 = -0.1629$, and $K_2 = 1.0615$. The corresponding coupling coefficients and external coupling can, therefore, be obtained as

$$\begin{aligned} k_{12} &= k_{34} = \frac{W}{\sqrt{g_1 g_2}} = 0.0436 \\ k_{23} &= K_2 \frac{W}{g_2} = 0.0384 \\ k_{14} &= K_1 \frac{W}{g_1} = -0.0085 \\ Q_{\text{ext}} &= \frac{g_1}{W} = 19.05. \end{aligned} \tag{7}$$

A few coupling configurations can be employed to realize the required coupling coefficients. Two such coupling structures, namely, configurations A and B, were discussed in Section III. Fig. 13 shows the coupling coefficients of configuration A, computed at 2.4 GHz, as a function of resonator separation Δx when

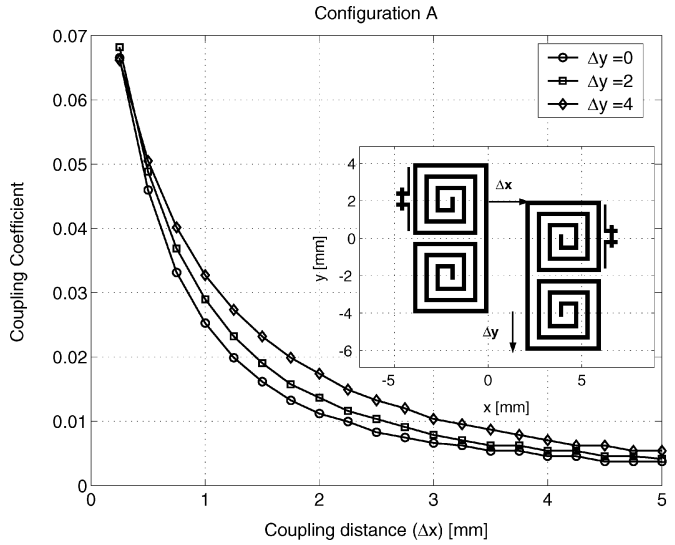

Fig. 13. Extracted coupling coefficients for configuration A as a function of resonator separation Δx for different values of vertical offsets Δy at 2.4 GHz.

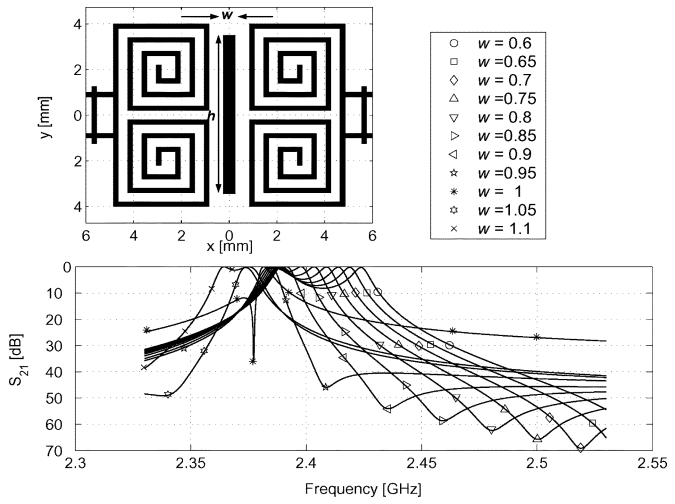

Fig. 14. Topology of the modified coupling configuration B and the effect of the width of slot incision (w) in the type and magnitude of coupling for the case of $h = 8$ mm.

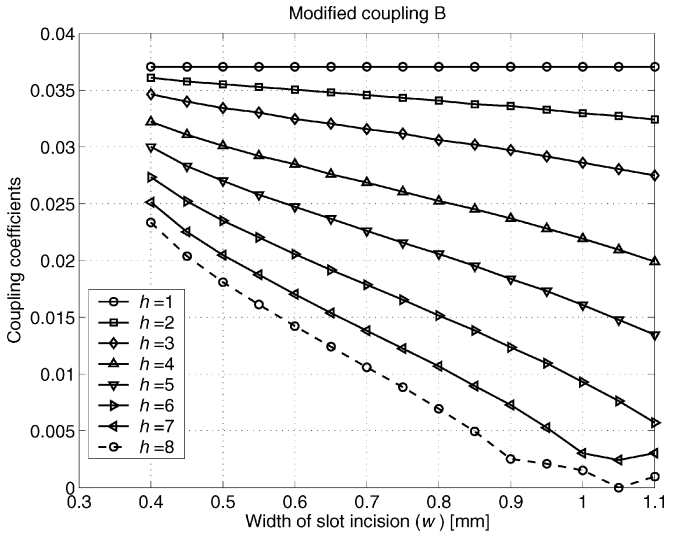

Fig. 15. Extracted coupling coefficients for the coupling configuration shown in Fig. 14 as a function of incision width and height (in millimeters) at 2.4 GHz.

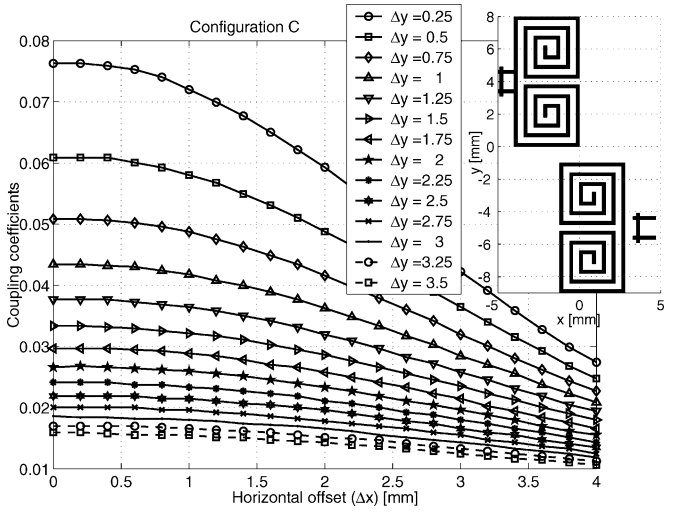

Fig. 16. Extracted coupling coefficients for coupling configuration C as a function of the horizontal offset between the resonators Δx for different values of vertical distances Δy at 2.4 GHz.

the vertical offset denoted by Δy is varied as a parameter. The nature of this coupling is, again, a dominantly magnetic mixed coupling.

A variation of configuration B, in which a short slot line is incised between the two resonators, was used in the second example of Section III. In Fig. 7, it was shown that, in configuration B, electric coupling is dominant. To reduce the coupling coefficient without increasing the distance between the resonators, a slot incision is again introduced between the two resonators, as illustrated in Fig. 14. This figure also shows the pole splitting in the transfer function with the incision width w as a free parameter. In these simulations the length of the incision is $h = 8$ mm. As the width of the incision increases, the electric coupling between the resonators decreases, and therefore, the net coupling is reduced. In Fig. 14, when $w = 1$ mm, a null appears approximately at the center frequency $\omega_n \approx \omega_0$, which implies that the electric and magnetic coupling are equal and totally cancel each other. Also as the incision width is increased, the frequency at which the null occurs falls below the center frequency $\omega_n < \omega_0$. This indicates that the dominant coupling becomes magnetic for larger values of incision width. Fig. 15 illustrates the coupling coefficients of the structure shown in Fig. 14 versus the incision width (w) when the incision height is varied as a free parameter. This structure, which will be referred to as modified configuration B, provides rather small values for electric coupling (negative coupling) without sacrificing the compactness of the structure.

Finally, coupling coefficients for configuration C are shown in Fig. 16 as a function of the horizontal offset (Δx) with the vertical distance Δy used as a parameter.This configuration is similar to the two previous structures with the exception that the offset parameters are much larger. This structure exhibits a dominantly magnetic coupling. Defining dominantly magnetic coupling by convention as positive coupling, and electric coupling as negative coupling, all the coupling coefficients, as required by (7) to synthesize a quasi-elliptic filter, can be realized.

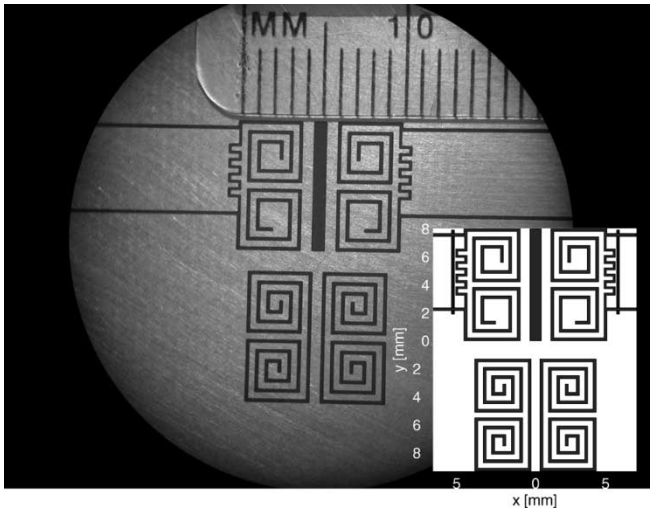

Fig. 17. Photograph and schematic layout of a miniaturized quasi-elliptic filter at 2.4 GHz with dimensions of $0.09\lambda_0 \times 0.14\lambda_0$.

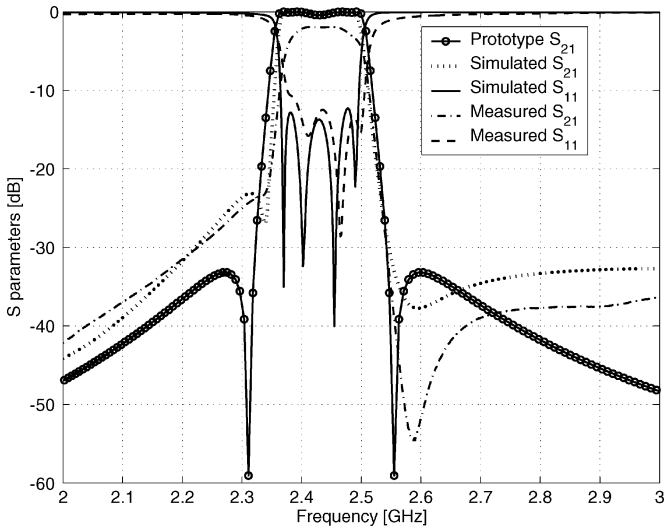

Fig. 18. Comparison between the lumped-element prototype, full-wave simulated, and measured S-parameters of the quasi-elliptic filter of Fig. 17.

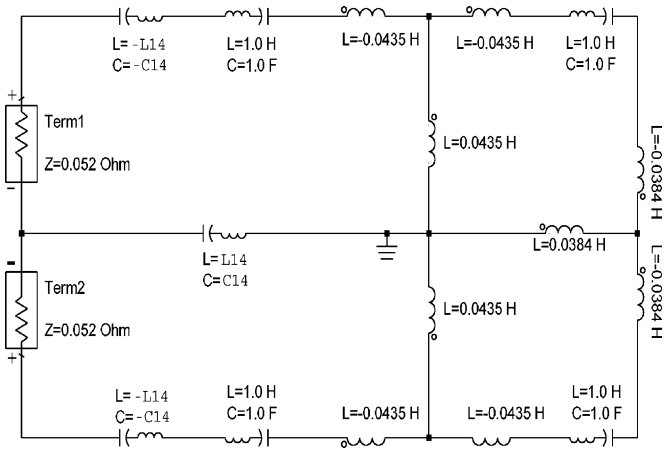

Fig. 19. Lumped-element prototype of a normalized quasi-elliptic bandpass filter in which the cross-coupling term k_{14} is realized by a mixed coupling where the difference between the two electric and magnetic coupling components is constant.

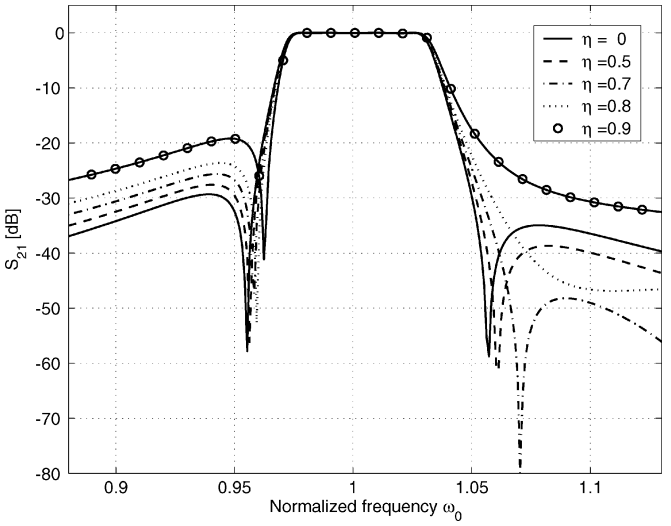

Fig. 20. Variation of the location of transmission zeroes of a normalized quasi-elliptic filter of Fig. 17 for different values of the ratio of the magnetic component to the electric component of the cross-coupling term $\eta = k_m/k_e$ given that $k_{14} = k_e - k_m$.

Fig. 17 shows the layout and photograph of this filter. This four-pole filter occupies an area as small as $0.09\lambda_0 \times 0.14\lambda_0$, while having an insertion loss of approximately 2.0 dB corresponding to the Q of 180. The Q of a straight half-wave microstrip resonator is approximately 170, but becomes much smaller when coiled. The simulated and measured responses are illustrated in Fig. 18, where very good agreement between the measurement and full-wave simulation is observed.

The locations of transmission zeros in the measurement, however, are not as predicted using the lumped-element prototype of Fig. 12. The asymmetry observed in the location of the transmission zeros can be attributed to the frequency dependence of the coupling coefficients [12]. The impedance inverter models, used in the low-pass prototype, assume a frequency-independent coupling, whereas the electric and magnetic couplings are frequency dependent in nature. In quasi-elliptic filters where both types of electric and magnetic couplings with opposite frequency dependence are present, the location of transmission zeroes can be shifted considerably. More importantly, in the proposed miniaturized design, the cross-coupling term, which controls the transmission zeros, is realized by subtracting two out-of-phase components of magnetic and electric couplings having different frequency dependence, resulting in an overall cross-coupling with a strong frequency dependence.

Fig. 19 shows the equivalent circuit of the normalized filter shown in Fig. 17, where the cross-coupling is realized by a dominantly electric mixed coupling. To ensure the proper value for the cross-coupling according to (7), the difference between the electric and magnetic has to be equal to k_{14}, i.e., $k_{14} = k_e - k_m = 1/C_{14}\omega_0 - L_{14}\omega_0$. Let $\eta = k_m/k_e < 1$ be the ratio of the magnetic component of the cross-coupling term to its electric component. Based on this definition, the value of the cross-coupling elements can be defined as $C_{14} = (1-\eta)/k_{14}$ and $L_{14} = \eta k_{14}/(1-\eta)$. Fig. 20 plots S_{21} of the equivalent circuit shown in Fig. 19 for different values of η, while keeping the net magnitude of the cross-coupling constant, namely, $k_{14} =$

0.0085. As seen in Fig. 20, the location of the transmission zero shifts when η is increased. The increase in η, while the overall cross-coupling term is fixed, indicates that a larger portion of the electric component of the cross-coupling is cancelled by an out-of-phase magnetic component. Obviously, the proper cancellation only takes place at the center frequency, but since the cross-coupling is frequency dependent, the coupling is more than required at frequencies above the passband and less below the passband. In order to alleviate the observed asymmetry in the location of transmission zeros and rejection band ripples, one might try to reduce η, which implies a smaller cancellation of the out-of-phase electric and magnetic couplings while maintaining the same value of k_{14}. As mentioned earlier, the required cross-coupling term needs to be rather small and can be realized by introducing a mixed electric–magnetic coupling in which the electric and magnetic couplings cancel each other out. To reduce the cancellation, and at the same time have the cross-coupling term remain intact, the absolute value of the electric coupling should be reduced using via-holes in the slot incision and/or increasing the vertical offset between the first and last resonators.

V. Conclusions

A new class of slot-line resonators for applications in miniaturized filter design have been demonstrated. The slot-line resonator offers flexibility of different coupling mechanisms, which facilitate various compact filter designs. It is shown that the resonators may be further miniaturized by increasing the value of inductive loading through increasing the number of turns in the coiled terminations with a moderate decrease in the resonator Q factor. The unloaded Q is higher than that of miniaturized microstrip filters of similar volume.

Both electric and magnetic couplings were demonstrated simply by positioning two such miniaturized resonators in different arrangements with respect to each other. A straightforward method was given to determine whether the coupling mechanism is magnetic or electric. A full-wave analysis was used to extract the coupling coefficients used in filter design.

To demonstrate the validity of the approach, three examples were studied including two four-pole Chebyshev filters, one of which used a mixed-coupling structure, and a four-pole quasi-elliptic filter. The agreement between the simulated and measured responses of these filters was shown to be excellent.

The prototype Chebyshev filters at 400 MHz with fractional bandwidths of 5% and 3% show insertion loss values of approximately 1.7 and 3.7 dB, while occupying a very small rectangular area $0.22\lambda_0 \times 0.06\lambda_0$ and $0.15\lambda_0 \times 0.06\lambda_0$, respectively. The unloaded Q of these filters is approximately three times greater than those of their microstrip counterparts.

A four-pole quasi-elliptic filter with $W = 5\%$ at 2.4 GHz was also fabricated, and its measured response was compared with numerical simulation. This filter with an improved out-of-band rejection gives 2-dB insertion loss while occupying a very small area of approximately $0.09\lambda_0 \times 0.14\lambda_0$. The effect of the frequency-dependent cross-coupling on the quasi-elliptic filter was also investigated.

Acknowledgment

The authors would like to thank Dr. R. Levy, R. Levy Associates, La Jolla, CA, for carefully reviewing this paper's manuscript and making very helpful suggestions.

References

[1] R. Levy, R. V. Snyder, and G. L. Matthaei, "Design of microwave filters," *IEEE Trans. Microwave Theory Tech.*, vol. 50, pp. 783–793, Mar. 2002.

[2] R. R. Mansour, "Microwave superconductivity," *IEEE Trans. Microwave Theory Tech.*, vol. 50, pp. 750–759, Mar. 2002.

[3] H. T. Su, F. Huang, and M. J. Lancaster, "Highly miniature HTS microwave filters," *IEEE Trans. Appl. Superconduct.*, vol. 11, pp. 349–352, Mar. 2001.

[4] P. Bradley, R. Ruby, J. D. Larson, Y. Oshmyansky, and D. Figueredo, "A film bulk acoustic resonator (FBAR) duplexer for USPCS handset applications," in *Proc. IEEE MTT-S Int. Microwave Symp. Dig.*, vol. 1, May 2001, pp. 367–370.

[5] A. Gopinath, A. F. Thomson, and I. M. Stephenson, "Equivalent circuit parameters of microstrip step change in width and cross junction," *IEEE Trans. Microwave Theory Tech.*, vol. MTT-24, pp. 142–144, Mar. 1976.

[6] M. Makimoto and S. Yamashita, "Compact bandpass filters using stepped impedance resonators," *Proc. IEEE*, vol. 67, pp. 16–19, Jan. 1979.

[7] E. G. Cristal and S. Frankel, "Hairpin-line and hybrid hairpin-line/half-wave parallel coupled-line filters," *IEEE Trans. Microwave Theory Tech.*, vol. MTT-20, pp. 719–728, Nov. 1972.

[8] M. Sagawa, K. Takahashi, and M. Makimoto, "Miniaturized hairpin resonator filters and their application to receiver front-end MIC's," *IEEE Trans. Microwave Theory Tech.*, vol. 37, pp. 1991–1997, Dec. 1989.

[9] S. Y. Lee and C. M. Tsai, "New cross-coupled filter design using improved hairpin resonators," *IEEE Trans. Microwave Theory Tech.*, vol. 48, pp. 2482–2490, Dec. 2000.

[10] J.-S. Hong and M. J. Lancaster, "Couplings of microstrip square open-loop resonators for cross-coupled planar microwave filters," *IEEE Trans. Microwave Theory Tech.*, vol. 44, pp. 2099–2109, Dec. 1996.

[11] ——, "Theory and experiment of novel microstrip slow-wave open-loop resonator filters," *IEEE Trans. Microwave Theory Tech.*, vol. 45, pp. 2358–2365, Dec. 1997.

[12] ——, "Aperture-coupled microstrip open-loop resonators and their applications to the design of novel microstrip bandpass filters," *IEEE Trans. Microwave Theory Tech.*, vol. 47, pp. 1848–1855, Sept. 1999.

[13] E. L. Mariani and J. P. Agrios, "Slot-line filters and couplers," *IEEE Trans. Microwave Theory Tech.*, vol. MTT-18, pp. 1089–1095, Dec. 1970.

[14] K. C. Gupta, P. Garg, I. Bahl, and P. Bhartia, *Microstrip Lines and Slotlines*, 2nd ed. Norwood, MA: Artech House, 1996.

[15] D. F. Williams and S. E. Schwarz, "Design and performance of coplanar waveguide bandpass filters," *IEEE Trans. Microwave Theory Tech.*, vol. MTT-31, pp. 558–566, July 1983.

[16] J. K. A. Everard and K. K. M. Cheng, "High-performance direct coupled bandpass filter on coplanar waveguide," *IEEE Trans. Microwave Theory Tech.*, vol. 41, pp. 1568–1573, Sept. 1993.

[17] M. Muraguchi, T. Hirota, A. Minakawa, K. Ohwada, and T. Sugeta, "Uniplanar MMIC's and their applications," *IEEE Trans. Microwave Theory Tech.*, vol. 36, pp. 1896–1901, Dec. 1988.

[18] T. Hirota, Y. Tarusawa, and H. Ogawa, "Uniplanar MMIC hybrids: A proposed new MMIC structure," *IEEE Trans. Microwave Theory Tech.*, vol. MTT-35, pp. 576–581, June 1987.

[19] T. Tsujiguchi, H. Matsumoto, and T. Nishikawa, "A miniaturized end-coupled bandpass filter using $\lambda/4$ hair-pin coplanar resonators," in *IEEE MTT-S Int. Microwave Symp. Dig.*, Baltimore, MD, June 1998, pp. 829–832.

[20] K. Yoshida, K. Sashiyama, S. Nishioka, H. Shimakage, and Z. Wang, "Design and performance of miniaturized superconducting coplanar waveguide filters," *IEEE Trans. Appl. Superconduct.*, vol. 9, pp. 3905–3908, June 1999.

[21] T. Tsujiguchi, H. Matsumoto, and T. Nishikawa, "A miniaturized double-surface CPW bandpass filter improved spurious response," *IEEE Trans. Microwave Theory Tech.*, vol. 49, pp. 879–885, May 2001.

[22] J. Sor, Y. Qian, and T. Itoh, "Miniature low-loss CPW periodic structures for filter applications," *IEEE Trans. Microwave Theory Tech.*, vol. 49, pp. 2336–2341, Dec. 2001.

[23] R. Azadegan and K. Sarabandi, "Miniaturized slot-line and folded-slot bandpass filters," in *IEEE MTT-S Int. Microwave Symp. Dig.*, Philadelphia, PA, June 2003, pp. 1595–1598.
[24] ——, "A novel approach for miniaturization of slot antennas," *IEEE Trans. Antennas Propagat.*, vol. 51, pp. 421–429, Mar. 2003.
[25] ——, "A compact planar folded-dipole antenna for wireless applications," in *Proc. IEEE AP-S Int. Symp.*, vol. 1, Columbus, OH, June 2003, pp. 439–442.
[26] E. Yuan and S. H. Chao, "Unloaded Q measurement: The critical-point method," *IEEE Trans. Microwave Theory Tech.*, vol. 43, pp. 1983–1986, Aug. 1995.
[27] *IE3D Electromagnetic Simulation and Optimization Package*, 9.0 ed., Zeland Software Inc., Fremont, CA, 2-2.
[28] G. L. Matthaei, L. Young, and E. M. T. Jones, *Microwave Filters, Impedance-Matching Networks and Coupling Structures*. New York: McGraw-Hill, 1964.
[29] A. E. Atia and A. E. Williams, "Narrow-bandpass waveguide filters," *IEEE Trans. Microwave Theory Tech.*, vol. MTT-20, pp. 258–265, Apr. 1972.
[30] R. Levy, "Filters with single transmission zeroes at real or imaginary frequencies," *IEEE Trans. Microwave Theory Tech.*, vol. MTT-24, pp. 172–181, Apr. 1976.
[31] K. T. Jokella, "Narrow-band stripline or microstrip filters with transmission zeroes at real and imaginary frequencies," *IEEE Trans. Microwave Theory Tech.*, vol. MTT-28, pp. 542–547, June 1980.

Reza Azadegan (S'98) was born in Tehran, Iran, in 1974. He received the B.S. degree from the Sharif University of Technology, Tehran, Iran, in 1996, the M.S. degree from the K. N. Toosi University of Technology, Tehran, Iran, in 1996, both in electrical engineering, and is currently working toward the Ph.D. degree in electrical engineering from The University of Michigan at Ann Arbor.

From 1997 to 1999, he was a Research Engineer with The Computational Electromagnetic Laboratory, Sharif University of Technology, where he was involved with the optimal design of reflector antennas using high-frequency techniques and genetic algorithms. He was also involved with the numerical modeling of the electromagnetic-wave propagation in optical waveguides. In Fall 1999, he joined The Radiation Laboratory, The University of Michigan at Ann Arbor. His research interests include design and miniaturization of planar antennas and microwave filters for wireless communication systems and microsensors.

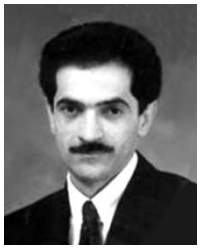

Kamal Sarabandi (S'87–M'90–SM'92–F'00) received the B.S. degree in electrical engineering from the Sharif University of Technology, Tehran, Iran, in 1980, and the M.S.E. and Ph.D. degrees from The University of Michigan at Ann Arbor, in 1986 and 1989, respectively, both in electrical engineering.

He is currently the Director of the Radiation Laboratory and a Professor with the Department of Electrical Engineering and Computer Science, The University of Michigan at Ann Arbor. His research areas of interest include microwave and millimeter-wave radar remote sensing, electromagnetic-wave propagation, and antenna miniaturization. He possesses 20 years of experience with wave propagation in random media, communication channel modeling, microwave sensors, and radar systems and is leading a large research group including two research scientists, ten Ph.D. and two M.S. students. Over the past ten years, he has generated 14 Ph.D. students. He was the Principal Investigator of many projects sponsored by the National Aeronautics and Space Administration (NASA), Jet Propulsion Laboratory (JPL), Army Research Office (ARO), Office of Naval Research (ONR), Army Research Laboratory (ARL), National Science Foundation (NSF), Defense Advanced Research Projects Agency (DARPA), and numerous industries. He has authored numerous book chapters and over 95 papers appearing in refereed journals on electromagnetic scattering, random media modeling, wave propagation, antennas, microwave-measurement techniques, radar calibration, inverse-scattering problems, and microwave sensors. He has also authored or coauthored over 200 papers and invited presentations in many national and international conferences and symposia on similar subjects. He is listed in *Who's Who in American Men and Women of Science*, *Who's Who in America*, and *Who's Who in Electromagnetics*.

Dr. Sarabandi is a vice president of the IEEE Geoscience and Remote Sensing Society (GRSS), chairman of the Awards Committee of the IEEE GRSS, and a member of the IEEE Technical Activities Board Awards Committee. He is the associate editor of the IEEE TRANSACTIONS ON ANTENNAS AND PROPAGATION and the IEEE SENSORS JOURNAL. He is also a member of Commission F of URSI and The Electromagnetic Academy. He was the recipient of the Henry Russel Award from the Regent of The University of Michigan (the highest honor the University of Michigan bestows on a faculty member at the assistant or associate level), the 1999 GAAC Distinguished Lecturer Award presented by the German Federal Ministry for Education, Science, and Technology, which is given to approximately ten individuals worldwide in all areas of engineering, science, medicine, and law, and a 1996 Teaching Excellence Award presented by the Electrical Engineering and Computer Science Department, The University of Michigan at Ann Arbor. Over the past several years, joint papers presented by his students at a number of symposia [IEEE Antennas and Propagation Society (IEEE AP-S) Symposia (1995, 1997, 2000, and 2001); the IEEE International Geoscience and Remote Sensing Symposium (1999); and the IEEE Microwave Theory and Techniques Society (IEEE MTT–S) International Microwave Symposium (IMS) (2001)] have been the recipients of Student Prize Paper Awards.